文章编号：1001－9014(2018)06－0657－06

DOI:10.11972/j.issn.1001－9014.2018.06.003

Numerical analysis of high radiation intensity dipole antenna arrays with terahertz chokes

CHEN Jing-Yuan[1,2], LIN Zhong-Xi[1], LIN Qi[1,2], XU Yu-Lan[1,2], SU Hui[1*]

(1. Fujian Institute of Research on the Structure of Matter, Chinese Academy of Sciences, Fuzhou 350002, China;
2. University of Chinese Academy of Sciences, Beijing 100049, China)

Abstract: To improve terahertz (THz) radiation intensity, the dipole antenna arrays with THz chokes on a thin LT-GaAs film are designed. The output radiation of the proposed linear array can be linearly enhanced by increasing the number of elements, while the average matching efficiency is changed insignificantly. The AC component flowing into the coplanar strip line (CPS) is limited by THz chokes which leads to a more stable resonant frequency, and the average matching efficiency is twice that of an array without chokes. We find the staggered array has a narrower emission spectrum than the gridding one due to the coupling of adjacent elements in the vertical direction. By designing the array on a polyimide lens instead of a silicon lens, a high input resistance can be obtained, and the total efficiency is raised from 25% to 35%.

Key words: terahertz dipole antenna array, LT-GaAs film, THz choke, high input resistance, polyimide lens, high radiation intensity

PACS: 84.40.Ba, 87.50.U-, 77.55.-g, 41.20.Jb

高辐射强度的带 THz 扼流圈的偶极天线阵列模拟分析

陈景源[1,2], 林中晞[1], 林 琦[1,2], 徐玉兰[1,2], 苏 辉[1*]

(1. 中国科学院福建物质结构研究所, 福建 福州 350002;
2. 中国科学院大学, 北京 100049)

摘要: 为了提高太赫兹辐射强度, 设计了带 THz 扼流圈的偶极天线阵列. 模拟结果表明, 增加直线阵的阵元数对平均匹配效率影响很小, 却能线性增加相干辐射强度. 加入 THz 扼流圈可减小进入到传输线的交流分量, 进而减小共振频率的偏移, 使平均匹配效率提升了两倍. 相比于网格排列的平面阵, 交错排列的阵元在垂直方向上具有更小的耦合, THz 发射谱更窄. 通过使用聚酰亚胺透镜代替硅透镜, 可有效提高输入电阻, 并将总效率由 25% 提高到 35%.

关 键 词: THz 偶极天线阵列; 低温砷化镓薄膜; THz 扼流圈; 高输入电阻; 聚酰亚胺透镜; 高辐射强度

中图分类号: TN822+.4　　**文献标识码**: A

Introduction

Terahertz (THz) technologies have shown remarkable development in recent years, and its applications have been proposed for biochemical tests, imaging and security systems[1-3]. High emission intensity terahertz sources play an important role in these applications. With their advantages of room temperature operation, wide tuning range and compactness, THz photomixers are considered as one of the most promising THz sources[4-5]. A typical THz photomixer is composed of a planar antenna integrated on a dielectric lens, which couples THz radiation into free space. A photomixer on a semiconductor substrate usually have a resistance above 10 kΩ, while the input resistance of the antenna is much lower than 10 kΩ, which leads to a serious impedance mismatch[6-11]. Thus, the impedance matching between photomixer and

Received date: 2018-03-08, **revised date**: 2018-08-24　　**收稿日期**: 2018-03-08, **修回日期**: 2018-08-24

Foundation items: Supported by National Natural Science Foundation of China (61405198), the National High-tech R&D Program (863 Program) (2013AA014202), the National Program on Key Basic Research Project (973 Program) (2016YFB0402300)

Biography: CHEN Jing-Yuan (1989-) male, Fuzhou, China, Ph. D. Research area involves THz antenna. E-mail: jingyuan10@126.com

* **Corresponding author**: E-mail: huisu@fjirsm.ac.cn

antenna become one of the key factors in improving the intensity of the THz radiation. Yang *et al*. investigated a logarithmic periodic antenna and got an input resistance of 1 kΩ at 72 GHz[7]. Nguyen and Ying designed antennas on the GaAs film, and they got the input resistance at 3 ~ 4 kΩ by reducing the effective permittivity[8-11]. However, a single terahertz antenna is susceptible to space electric field shielding caused by space charge and radiation field from high excitation densities of lasers[12-14]. Therefore, we report here a scheme of dipole antenna arrays which simultaneously provide high input resistance and high average matching efficiency, and thus improve the total efficiency of converting the THz photocurrent into the THz radiation.

In this paper, we use a commercial software Computer Simulation Technology (CST) Microwave Studio package to investigate performance of THz photomixer arrays. In Sect. 1, we propose the design of the antenna array. In Sect. 2, we discuss the effects of the arrays' structure, parameters and arrangement on the input resistance and matching efficiency of the THz photomixer. In Sect. 3, we compare the radiation pattern of antenna array on both silicon and polyimide tended hemispherical lens. By comparing the interference field of THz arrays on polyimide and silicon lens respectively, we demonstrate the superiority of the antenna array on the polyimide lens with THz chokes in transferring THz photocurrent into a radiated THz wave in Sect. 4.

1 Dipole antenna array structure

A dipole antenna with THz chokes has higher input resistance in Ref. [10], but it has a size of 230 μm × 1 200 μm for owning many THz chokes. It is too large to form an array. So, we reduce the amount of THz chokes and share the coplanar strip line (CPS) when designing the array. The geometry of a three-element linear array is shown in Fig. 1, and its parameters are shown in Table 1. As the basic element, the dipole antenna transfers photocurrent into linear polarized THz radiation. The label P1, P2 and P3 represent the gaps of dipole antennas which are illuminated by laser beams. A THz choke with a width of B is located between two adjacent elements, which can dampen the AC component propagating along the CPS and increase the input resistance at resonance frequency[8-11,15]. Between the DC bias sources and the elements at the edge, there are more than three THz chokes with a distance of F. The CPS with a width of e and a length of $2L = 1\,900$ μm provides theDC bias for the dipole antennas. In simulation, three discrete S-parameter ports are used to excite above gaps with signals in phase. The impedance of each of the three ports is set to 10 kΩ, respectively. In order to match practical situations, we use Gaussian-shape pulse signals to find the resonant frequency, and then, the CW sinusoidal signals in the resonant frequency is selected to excite the radiation field.

The antenna array is made of a 0.5 μm-thick Au film, which has a conductivity of 1.6×10^7 S/m. Below the Au film, there is a cylinder LT-GaAs ($\varepsilon_{GaAs} = 12.9$) substrate with a radius of $R = 1\,000$ μm and a thickness of d. Because the input resistance has a negative correlation with substrate's effective permittivity $\sqrt{\varepsilon_{eff}}$, a 5 μm thick substrate is chosen to get a higher input resistance[8-11].

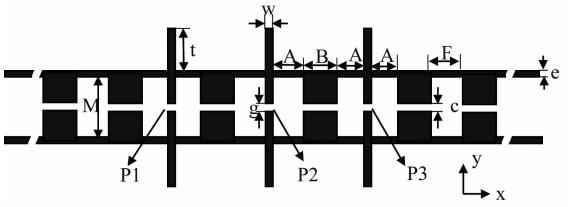

Fig. 1 Geometry of a three-element linear array
图1 三元直线阵结构示意图

Table 1 Design parameters of the antenna array
表1 天线阵列的参数尺寸

Parameter	*A*	*B*	*c*	*t*	*F*	*M*	*e*	*w*	*g*
Value/μm	30	30	2	16	30	30	2	2	5

2 Results and analysis

2.1 The linear array

We analyze the input resistance of linear array along the x axis. Figure. 2 shows the impedance characteristics of the three-element linear array. The resonant frequency is found at 0.926 THz, with the imaginary parts of impedance tend to zero and the real parts reach to the peak. Since the antenna structure is symmetrical, the input resistance of the P1 and P3 can be considered complete equal. The input resistance of the P2 is 1.6 times higher than that of the P1. Figure 3 illustrates the change of input resistance with the increasing of antenna number n from 1 to 4. We find the increment of the number of elements leads to a little shift of resonance frequency. Compared with a single antenna, the input resistances of the elements in the middle of linear array increase, while those at the edges of the linear array decrease. Because the element in different location has different input resistance, it is difficult to evaluate the array's characters using series of value. For simplicity, we use the average matching efficiency ($\bar{\eta}_n$) at resonant frequency to characterize the performance of the n-element array. The matching efficiency of a single antenna is given by[8]

$$\eta = 1 - \left(\frac{Z_a - Z_p}{Z_a + Z_p}\right)^2 \quad , \quad (1)$$

where Z_a is the input resistance of the antenna; Z_p is set to 10 kΩ which represents the impedance of the photomixer. The average matching efficiency of n-element array can be expressed as:

$$\bar{\eta}_n = \frac{1}{n}\sum_{i=1}^{n}\eta_{n,i} \quad . \quad (2)$$

We calculated the matching efficiency of every element in an n-elements array, then calculated their average value. The average matching efficiencies of the linear arrays with n from 1 to 4 are $\bar{\eta}_1 = 77.3\%$, $\bar{\eta}_2 = 72.6\%$, $\bar{\eta}_3 = 74.9\%$, and $\bar{\eta}_4 = 73.4\%$, respectively. It shows that the number of elements has only a little influence on the average matching efficiency in the linear array. We can improve the output radiation by simply increasing the number of elements.

In order to study the effect of THz chokes in a linear array, we compare the difference between the linear array with and without THz choke. Based on Fig. 1, we remove all THz chokes and get a traditional linear array. The resonant frequency of the linear array without THz choke rise to 1.16 THz without changing other parameters. To make the resonant frequency of these two different arrays closer, the parameter M of linear array without THz choke is alter from 30 μm to 65 μm. Table 2 lists the average matching efficiency and resonant frequency of two different linear arrays. It is found that the average matching efficiency of the linear array with THz choke is twice more than that of the linear array without THz choke. And even the number of elements of linear array increase to 9, the the average matching efficiency still over 72%. This confirms the former conclusion about the relationship between n and $\bar{\eta}_n$. The resonant frequency of the former array increases with the number of element, while the latter one is not regular. This difference is due to the fact that the addition of THz choke restricts the AC component in space, and the current distribution becomes more cyclical, thus leads to a more stable resonant frequency. Figure 4 explains the surface current distribution of three-element linear array at the resonant frequency. It is clear that the surface current is limited by the THz choke, and almost no transmission along the CPS. Although the elements in a linear array share the same CPS, they have little influence on each other.

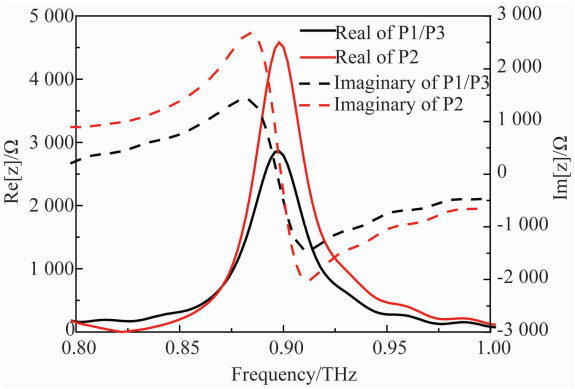

Fig. 2　Input resistance of three-element linear array
图 2　三元直线阵的输入电阻

Table 2　Average matching efficiency $\bar{\eta}_n$ and resonant frequency of linear array with THz chokes and without THz chokes while n from 3 to 9

表 2　阵元数从 3～9 时，带 THz 扼流圈和无 THz 扼流圈直线阵的平均匹配效率和共振频率

n	with THz choke		without THz choke	
	$\bar{\eta}_n$	Resonant frequency	$\bar{\eta}_n$	Resonant frequency
3	74.9%	0.898 THz	29.4%	0.929 THz
4	73.4%	0.902 THz	30.7%	0.928 THz
5	72.0%	0.906 THz	30.6%	0.931 THz
6	72.1%	0.908 THz	30.6%	0.916 THz
7	72.3%	0.910 THz	33.8%	0.930 THz
8	72.0%	0.912 THz	32.0%	0.918 THz
9	72.8%	0.914 THz	34.2%	0.923 THz

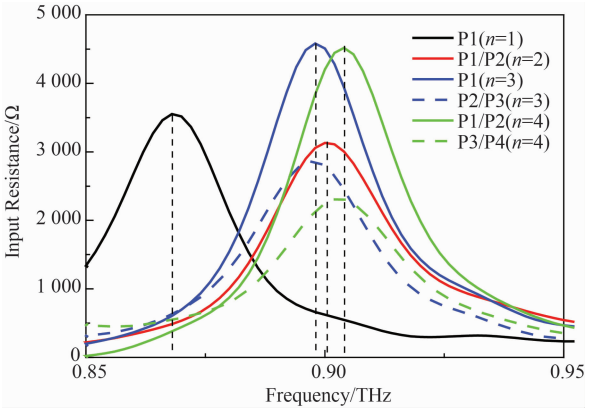

Fig. 3　Input resistance of linear array with different number of elements
图 3　不同阵元数下直线阵的输入电阻

Fig. 4　Surface current distribution of three-element linear array at resonant frequency
图 4　三元直线阵在共振时的表面电流分布图

2.2　Planar array

Considering the exciting laser beam always has a Gaussian distribution rather than linear, we investigate two planar arrays with different arrangement. Figure 5 presents two shape of array, (a) gridding planar array has the same three-element linear array in all rows and aligned in the vertical direction; b) staggered planar array has different linear array in different rows and elements in adjacent rows are staggered. Two planar arrays are both symmetrical to guarantee the interference fields of the array are mainly located on the z-axis. From Figure 6, we find the resonant peaks are staggered in both kind of array. The first (red color) and third (blue color) rows of array share the same resonant peak, while the second row (green color) has a separated peak. The distance of the staggered formant in two arrays are $\Delta f_{\text{gridding}} = 0.024$ THz and $\Delta f_{\text{staggered}} = 0.02$ THz, respectively. The structure of each row is exactly the same in the gridding planar array which should have the same characteristic. But the coupling of adjacent elements in the vertical direction causes the separation of resonant peaks. On the contrary, the staggered planar array has staggered adjacent elements in the vertical direction, which leads to less coupling to each other. Table 3 lists the Δf of two planar arrays with different thickness of the substrate. It shows that the Δf varies with the thickness, yet it is difficult to eliminate the Δf by adjusting the parameters of different rows. The staggered planar array has a narrower emission spectrum due to smaller Δf, which means it is a better configuration for higher radiation intensity. However, its average matching efficiency is 59.1% at 0.910 THz, which is about 13% lower than that of the linear array. And the average matching efficiencies of gridding planar array with different amount of elements are $\bar{\eta}_{2\times2}$ =

57%, $\bar{\eta}_{3\times3}$ = 50%, $\bar{\eta}_{4\times4}$ = 47%, $\bar{\eta}_{5\times5}$ = 47% respectively. When we add more elements, there are more separate resonant peaks which cause a smaller average matching efficiency.

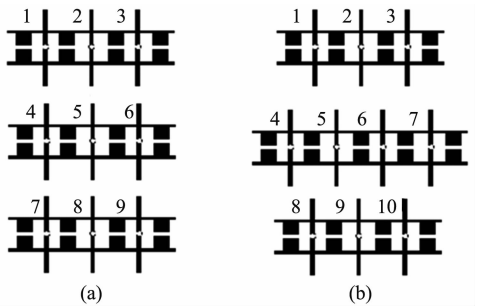

Fig. 5 Two planar arrays and the sequence of elements (a) gridding planar array, and (b) staggered planar array

图5 两种不同排列方式的平面阵及阵元标号(a)网格排列,(b)交错排列

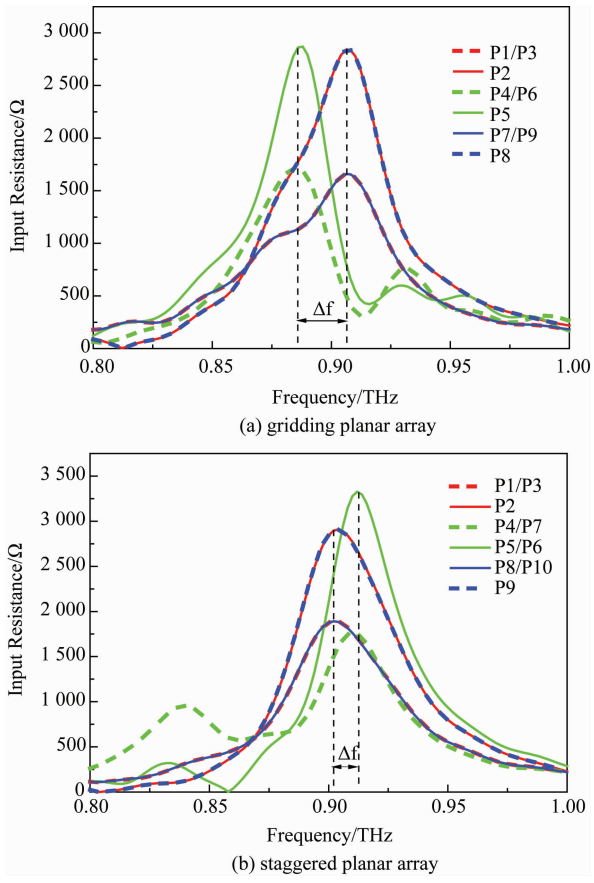

Fig. 6 Input resistance of two planar arrays (a) gridding planar array, and (b) staggered planar array

图6 两种不同排列方式的平面阵输入电阻(a)网格排列,(b)交错排列

3 Radiation pattern

For practical application, a silicon lens is often used to collimate the THz radiation, which however seriously reduces the input resistance due to the high permittivity.

Table 3 The Δf of two different planar arrays at different thickness of substrate

表3 两种不同排列方式的平面阵在不同衬底厚度下的谐振峰频差 Δf

Thickness of substrate/μm	$\Delta f_{gridding}$/THz	$\Delta f_{staggered}$/THz
5	0.024	0.002
15	0.01	0.006
25	0.01	0.008
35	0.011	0.008
45	0.019	0.007
55	0.043	0.017
65	0.005	0.005

To overcome this, Nguyen and Ying designed some structures without reducing the input resistance[8-11]. But these structures are very difficult to fabricate. In this paper, we provide an easy-fabricating structure to mitigate the impact of this shortcoming. The silicon (ε_r = 11.9, loss free) lens is replaced by polyimide (ε_r = 3.5, loss tangent = 0.002 7) lens, which has lower permittivity and less effect on input resistance. It is preferable to transfer the LT-GaAs film to a polyimide lens by epitaxial lift-off method[12,16]. In addition, the total internal reflection of THz radiation rarely occur in a thin LT-GaAs film, so it is not necessary to use a silicon lens with high permittivity to couple the THz beam into free space[17]. For comparison, both polyimide and silicon lens are simulated, with the same extended hemispherical structure (R = 1 000 μm, L = 0.5R)[8,18]. Figure 7 illustrates the radiation pattern of staggered array with a polyimide lens at 0.841 THz (red color) and with a silicon lens at 0.753 THz (green color). Radiation energy is concentrated on the side of hemispherical lens, with the directivity of 16.9 dBi and 19.2 dBi, respectively. Although silicon lens has higher directivity than polyimide lens, yet the input resistance drops more due to larger permittivity, as shown in Fig. 8. Low input resistance means

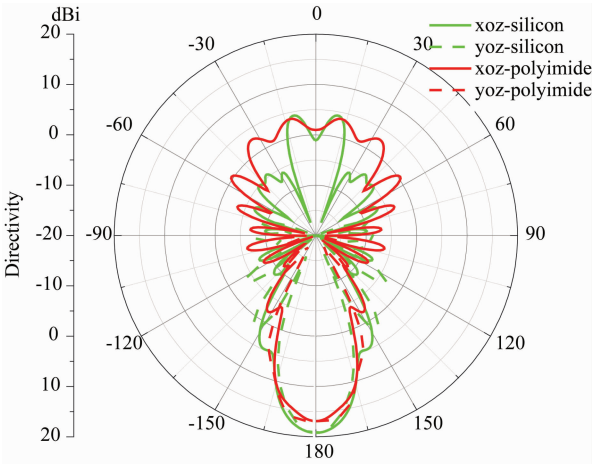

Fig. 7 Radiation patterns of the staggered array with a polyimide lens at 0.84 THz (red color) and with a silicon lens at 0.753 THz (green color)

图7 使用不同透镜时谐振频率处交错排列平面阵的辐射方向图(红色为聚酰亚胺透镜,0.84 THz;绿色为硅透镜,0.753 THz)

high mismatch, the average matching efficiency of silicon lens is only 44.8%, compared with 51.1% of polyimide lens. Thus the total efficiency is raised from 25% to 35% after replacing the silicon lens by polyimide lens.

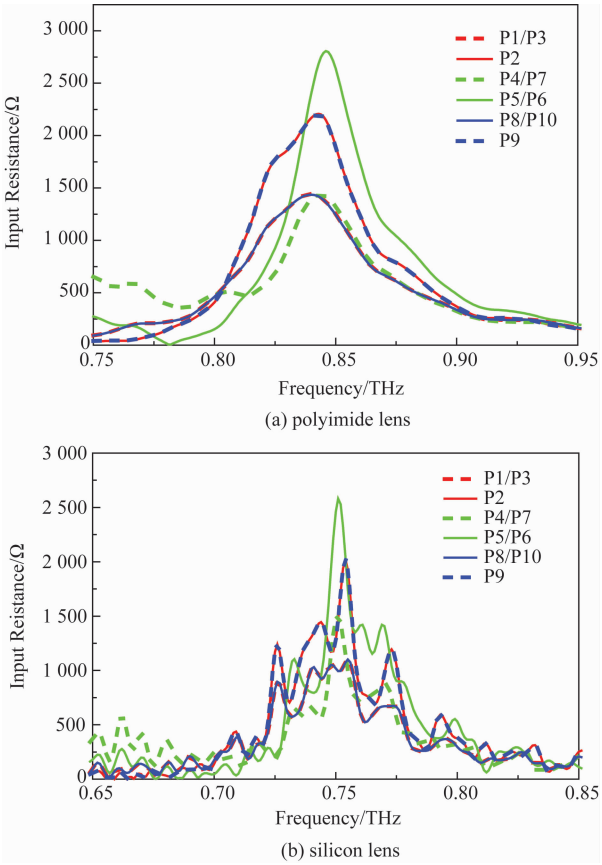

Fig. 8　Input resistance of staggered array with (a) a polyimide lens, (b) a silicon lens

图 8　使用不同透镜时交错排列平面阵的输入电阻(a)聚酰亚胺透镜,(b)硅透镜

4　Interference field intensity

We examine the interference field of the above arrays and compare their performance in transferring THz photocurrent into a radiated THz wave. Considering the above arrays are symmetrical, the interference field intensity $E(t)$ can be monitored by a far-field E-probe located on the -z-axis with a distance of 10 000 μm. When excited by a light source, the THz photomixer generates both sinusoidal AC and DC photocurrent[1]. Because DC component do not contribute to THz radiation, the sinusoidal signals last for 30 ps in phase are used to excite the elements of array in simulation. The frequency of sinusoidal signals is equal to the resonant frequency of the array. Figure 9 reveals the interference field intensity $E(t)$ of a three-element linear array. The amplitude of field intensity increases after being resonant amplified, and finally reaches to maximum E_{peak} in a steady state. We record the E_{peak} of all above arrays with different number of elements in Fig. 10. From it, we are convinced that most arrays proposed in this paper have better performance than the arrays without chokes. As discuss in Sect. 4, a polyimide lens is a super choice for coupling THz wave into space. The interference field intensity is linear with number of elements for the linear arrays, which proves that the output radiation of the proposed linear array can be promoted by simply increasing the number of elements. Compared to pulse radiation of THz photoconductive antenna arrays[12-14], the continuous radiation of photomixer arrays has stronger coherent enhancement results. The main reasons include frequency singleness, thin LT-GaAs film and closer distance between elements. These designed arrays are promising to achieve high field intensity with more sophisticated experiments satisfying the ideal condition.

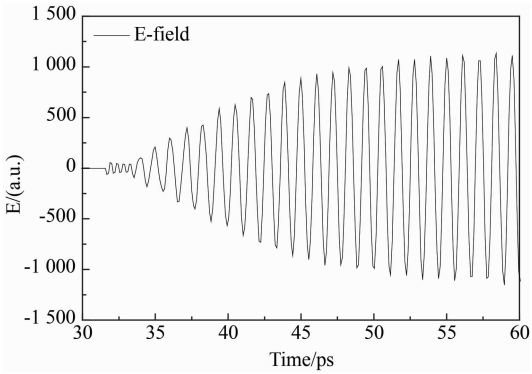

Fig. 9　The interference field intensity $E(t)$ of a three-element linear array

图 9　三元直线阵的辐射相干场强 $E(t)$

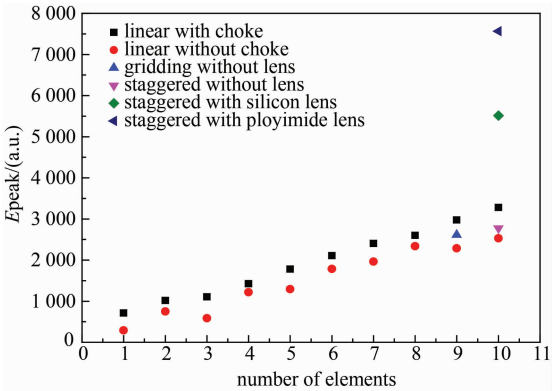

Fig. 10　E_{peak} of all above arrays with different number of elements

图 10　文中所提及的天线阵的相干场强的峰值 E_{peak} 与阵元数的关系

5　Conclusion

Terahertz dipole antenna arrays with THz chokes on the thin LT-GaAs film are presented in this paper. We analyze the radiation characteristics of different antenna array. In the linear array we find the number of elements only shift the resonant frequency slightly and has little effect on the input resistance and the average matching efficiency. Because the THz chokes restrict the AC component into the bias line, thus the average matching efficiency of the linear dipole array with THz chokes is more

than doubling that of the array without chokes. In planar structure, the staggered array has a narrower emission spectrum than the gridding ones because of avoiding the coupling of adjacent elements in the vertical direction. To improve the coupling of THz radiation, we replace the high-permittivity silicon lens by a low-permittivity polyimide lens to reduce negative impact on the input resistance, and the total efficiency raise from 25% to 35%. By examining the interference field of THz arrays excited by continuous sinusoidal signals in phase, we prove the superiority of the antenna array on the polyimide lens with THz chokes in transferring THz photocurrent into a radiated THz wave.

References

[1] Lee Y S. *Principles of terahertz science and technology*[M]. New York: Springer US, 2009.

[2] Federici J F, Schulkin B, Huang F, *et al*. THz imaging and sensing for security applications—explosives, weapons and drugs [J]. *Semiconductor Science and Technology*, 2005, **20**(7): S266 - S280.

[3] Jarrahi M. Advanced photoconductive terahertz optoelectronics based on nano-antennas and nano-plasmonic light concentrators [J]. *IEEE Transactions on Terahertz Science and Technology*, 2015, **5**(3): 391 - 397.

[4] Brown E R, Mcintosh K A, Nichols K B, *et al*. Photomixing up to 3.8 Thz in low-temperature-grown GaAs [J]. *Applied Physics Letters*, 1995, **66**(3): 285 - 287.

[5] Matsuura S, Ito H. *Generation of CW terahertz radiation with photomixing*[M]. Berlin Heidelberg: Springer, 2005: 157 - 202.

[6] Kamran E, Thomas K-O, Koch M. Numerical simulation of photoconductive dipole antennas: the effect of the dc bias striplines[C]. In 16th International Symposium On Space Terahertz Technology, 2005: 305 - 308.

[7] Yang S Y, Cho C S, Lee J W, *et al*. Design of sub-THz log-periodic antenna for high input impedance[C]. In International Conference on Infrared, Millimeter, And Terahertz Waves, 2009: 1 - 2.

[8] Nguyen T K, Han H, Park I. Full-wavelength dipole antenna on a hybrid GaAs membrane and Si lens for a terahertz photomixer [J]. *Journal of Infrared, Millimeter, and Terahertz Waves*, 2012, **33**(3): 333 - 347.

[9] Han K, Nguyen T K, Park I, *et al*. Terahertz yagi-uda antenna for high input resistance [J]. *Journal of Infrared, Millimeter, and Terahertz Waves*, 2009, **31**(4): 441 - 454.

[10] Nguyen T K, Han H, Park I. Numerical study of a full-wavelength dipole antenna on a GaAs membrane structure at terahertz frequency [J]. *Journal of Infrared, Millimeter, and Terahertz Waves*, 2011, **32**(6): 763 - 777.

[11] Yin W, Kennedy K, Sarma J, *et al*. A photomixer driven terahertz dipole antenna with high input resistance and gain [J]. *Progress In Electromagnetics Research M*, 2015, **44**: 13 - 20.

[12] Awad M, Nagel M, Kurz H, *et al*. Characterization of low temperature GaAs antenna array terahertz emitters [J]. *Applied Physics Letters*, 2007, **91**(18): 181124.

[13] LIU Qing-Yi., CHENG Ping, LAN Li-Tao, *et al*. Study on power combination of terahertz photoconductive antenna array [J]. *Optoelectronic Technology*(刘青宜,程萍,兰立涛,等. 太赫兹光导天线阵列功率空间合成规律研究. **光电子技术**), 2014, **34**(04): 244 - 249.

[14] Berry C W, Hashemi M R, Jarrahi M. Generation of high power pulsed terahertz radiation using a plasmonic photoconductive emitter array with logarithmic spiral antennas [J]. *Applied Physics Letters*, 2014, **104**(8): 081122.

[15] Duffy S M, Verghese S, Mcintosh A, *et al*. Accurate modeling of dual dipole and slot elements used with photomixers for coherent terahertz output power [J]. *IEEE Transactions On Microwave Theory And Techniques*, 2001, **49**(6): 1032 - 1038.

[16] GUO Chun-Yan, XU Jian-Xing, PENG Hong-Ling, *et al*. Study of process for epitaxial layer transfer of on-chip thz antenna integrated device [J]. *Journal of Infrared and Millimeter Waves*(郭春妍, 徐建星, 彭红玲,等 片上太赫兹天线集成器件 LT-GaAs 外延转移工艺. **红外与毫米波学报**), 2017, **36**(02): 220 - 224 + 234.

[17] Khiabani N. Modelling, design and characterisation of terahertz photoconductive antennas[J]. *Computers & Mathematics with Applications*, 2013, **64**(6): 1567 - 1574.

[18] Filipovic D F, Gearhart S S, Rebeiz G M, *et al*. Double-slot antennas on extended hemispherical and elliptical silicon dielectric lenses[J]. *IEEE Transactions on Microwave Theory and Techniques*, 1993, **41**(10): 1738 - 1749.